Circular Dichroism and Electron Microscopy of a Core Y61F Mutant of the F1 Gene 5 Single-Stranded DNA-Binding Protein and Theoretical Analysis of CD Spectra of Four Tyr → Phe Substitutions†

Teresa M. Thompson,‡ Barbara L. Mark,‡ Carla W. Gray,*,‡ Thomas C. Terwilliger,§ Narasimha Sreerama,|| Robert W. Woody,*,|| and Donald M. Gray*,‡

Department of Molecular and Cell Biology, Mail Station FO31, The University of Texas at Dallas, Box 830688, Richardson, Texas 75083-0688, Genomics and Structural Biology, Life Sciences Division, Mail Stop M880, Los Alamos National Laboratory, Los Alamos, New Mexico 87545, and Department of Biochemistry and Molecular Biology, Colorado State University, Fort Collins, Colorado 80523

Received October 14, 1997; Revised Manuscript Received March 20, 1998

ABSTRACT: A core Y61F mutant of the gene 5 single-stranded DNA-binding protein (g5p) of f1 bacterial virus aggregated when expressed from a plasmid, but, after refolding in vitro, it behaved much like wild-type and may be a stability or folding mutant. Circular dichroism (CD) titrations showed the same cooperative polynucleotide binding modes for Y61F and wild-type g5p. There are $n = 4$ and $n \cong 2.5$ modes for binding to poly[d(A)] at low ionic strengths, but $n = 4$, $n = 3$, and $n \cong 2-2.5$ modes for binding to fd single-stranded viral DNA (fd ssDNA), where n is the number of nucleotides occluded by each bound g5p monomer in a given mode. Y61F g5p has slightly reduced affinity in the $n = 4$ mode. Electron microscopy showed that Y61F g5p forms left-handed nucleoprotein superhelices indistinguishable from wild-type. Progression from binding to fd ssDNA in the $n = 4$ to $n = 3$ to $n \cong 2-2.5$ mode is accompanied by an increase in the number of helical turns, an increase from (7.7 ± 0.3) to (9.5 ± 0.3) to (∼10−13) g5p dimers per turn, and a decrease in the number of DNA nucleotides per turn. From CD spectra for four of five possible Y → F g5p mutants, we infer that the fifth tyrosine, Tyr 56, contributes strongly to the CD. Retention of a strong 229 nm CD band in all mutants indicates that all retain elements of the native structure. Spectra of Y26F, Y34F, and Y61F g5p imply limited mobility of the replacement Phe. Comparison of measured with calculated CD spectra also suggests limited mobility for Tyr 26 and Tyr 34 in g5p in solution, and provides new information that the g5p structure in solution may be dominated by Tyr 41 rotamers differing from that stabilized in the crystal.

The Ff [1] gene 5 protein (g5p) is an extensively studied single-stranded DNA-binding protein that is widely regarded as a model from which principles for nonsequence-specific interaction of proteins with single-stranded DNAs may be elucidated. Identical Ff g5p molecules are encoded by the closely related f1, fd, and M13 filamentous bacterial virus strains (collectively designated Ff viruses) that infect *Escherichia coli.* The g5p binds to nascent viral ssDNA, sequestering the genomic DNA and organizing it as a nucleoprotein complex that is a precursor for virus assembly (*1*). The two DNA-binding sites on each dyadic g5p dimer bind to oppositely-oriented segments of ssDNA, and the g5p folds the ssDNA back on itself so that two single DNA strands run in opposite directions in complexes with cooperatively bound g5p dimers (*2*, *3*). Electron microscopy and electron diffraction showed that complexes of g5p with the circular fd viral ssDNA consist of a single-start, flexible nucleoprotein helix (*4*), and electron microscopy yielded proof of a left-handed helical structure (*5*, *6*). Neutron diffraction and X-ray scattering showed that the path of the single-stranded DNA is along the interior surface of the protein helix (*6*, *7*). Cooperativity, in this system, is thought to involve protein−protein binding interactions between adjacent g5p dimers bound to ssDNA, so that a series of

† CD spectroscopy of Y61F g5p was performed by T.M.T. in partial fulfillment of the requirement for the M.S. degree in the Program in Molecular & Cell Biology at the University of Texas at Dallas. Supported by NSF Grant MCB-9405683 and Robert A. Welch Foundation Grant AT-503 (to D.M.G.), and by NIH Research Grants GM22994 (R.W.W.), GM38714 (T.C.T.), and GM34293 (C.W.G.).

* Corresponding authors for electron microscopy (cwgray@utdallas.edu), theoretical CD (rww@lamar.ColoState.edu), and experimental CD (dongray@utdallas.edu).

‡ The University of Texas at Dallas.

§ Los Alamos National Laboratory.

|| Colorado State University.

[1] Abbreviations: Ff, group name for the fd, f1, and M13 strains of filamentous bacterial viruses; g5p, identical gene 5 single-stranded DNA-binding proteins encoded by any of the Ff viruses; fd ssDNA, single-stranded circular genomic DNA of fd virus; ssDBP, single-stranded DNA-binding protein; n, the number of nucleotides occluded by each g5p monomer in one of the protein's stoichiometric binding modes; $K_{int}\omega$, product of the symmetry-corrected intrinsic association constant K_{int} and the cooperativity factor ω, for binding of g5p dimers to polynucleotides (defined in Experimental Procedures); EM, electron microscopy; CD, circular dichroism; $\epsilon_L - \epsilon_R$, difference in molar absorption coefficients for left- vs right-circularly polarized light; poly[d(A)], polymer of deoxyriboadenylic acid; *P*/*N* ratio, molar ratio of g5p monomers to nucleotides; DBM, Debye−Bohr magneton, a unit of rotational strength equal to 0.9273×10^{-38} cgs units; PDB, Brookhaven Protein Data Bank; rmsd, root-mean-square deviation.

S0006-2960(97)02545-2 CCC: $15.00
Published on Web 04/30/1998

interacting dimers form a protein helix that determines the path followed by the two strands of bound ssDNA (*5*, *8*).

The crystal structure of the Ff g5p has been determined to 1.8 Å resolution (*8*). The g5p monomer consists of a five-β-strand OB fold motif (*9*) that is shared not only with the closely related ssDBP of filamentous bacteriophage Pf3 but also with the ssDNA-binding domain of human replication protein A (RPA) and the anticodon-binding domain of yeast aspartyl tRNA synthetase (*10*−*12*). The Ff g5p monomer is a multifunctional but compact structure, consisting of only 87 amino acids. Its aromatic residues include five functionally diverse Tyr, three Phe, and no Trp. The five Tyr of the Ff g5p are conserved, or conservatively replaced by Phe, in the sequences and structures of the related ssDBPs encoded by IKe and Pf3 filamentous bacterial viruses (*11*, *13*, *14*). Three of the Tyr (Tyr 26, 34, 41) of Ff g5p reside on the protein surface. Tyr 26 appears to stack with DNA bases (*15*, *16*), and Tyr 41 is probably involved in cooperative interactions between neighboring g5p dimers bound to ssDNAs (*8*, *16*−*19*). Tyr 34 is also near the proposed dimer−dimer interface in the helix of g5p dimers as modeled by Skinner et al. (*8*). Tyr 56 and Tyr 61, on the other hand, are largely buried in the interior of the g5p.

This communication is part of an effort to determine the functional and CD spectral properties of the five g5p tyrosines, using mutants in which the tyrosines are substituted by other residues. Mark et al. (*20*) recently characterized the CD spectra and binding properties of the surface Tyr → Phe mutants Y26F, Y34F, and Y41F. The present report is the first study by CD and electron microscopy of a g5p mutant, Y61F, having a Phe substituted for a Tyr that is largely buried. Many nonsurface g5p residues are intolerant to substitution, which produces nonfunctional g5p mutant proteins (*21*). A number of g5p mutants, including Y61H, have shown a tendency to denature and aggregate, and Y61H and Y61S g5p mutants have biological activity ("packaging inhibition") that is reduced in comparison with that of the wild-type g5p (*18*, *22*).

The Y61F g5p is produced as an insoluble aggregate when expressed from a plasmid in *E. coli*. After refolding the Y61F g5p in vitro, we used CD analysis of binding behavior and electron microscopy of the complexes as sensitive tests of functional integrity. Wild-type g5p binds to polynucleotides in multiple interactive modes, such that each bound g5p monomer occludes a different number of nucleotides, *n*, in the different modes (*20*, *23*, *24*). The value of *n* should be an integer if each g5p interacts with a set of nucleotides in the same manner. The wild-type g5p binds in a single $n \cong 4$ mode to fd ssDNA and DNA homopolymers at 0.06−0.1 M NaCl (*20*, *23*, *25*, *26*). At lower ionic strengths, however, binding also occurs in weaker secondary and tertiary modes, so that the g5p binds to poly[d(A)] in two modes ($n = 4$ and $n \cong 2.5$) and to fd ssDNA in three modes ($n = 4$, $n = 3$, and $n \cong 2-2.5$) (*20*, *23*, *26*, and this communication). Although the primary $n = 4$ mode should predominate at physiological ionic strengths, the secondary modes may become significant at the high concentrations of g5p (*27*) that occur in vivo.

We find that the Y61F g5p has substantially normal properties after being refolded in vitro. The binding modes and structures of the complexes formed by Y61F g5p are indistinguishable from complexes with wild-type g5p, and the binding affinity of the Y61F g5p in the $n = 4$ mode is only slightly reduced.

The small size of the Ff g5p and its rich endowment of functionally important Tyr and Phe aromatic residues make the g5p and its site-directed mutants well suited for studies relating protein CD spectral characteristics to the known spatial arrangement of the amino acids in the g5p. In the Ff g5p, spectral contributions in the 250−300 nm aromatic region are less complicated than at shorter wavelengths where multiple peptide contributions are present; however, the 205−250 nm region is dominated by the 229 nm tyrosyl CD band that is perturbed upon binding to ssDNA (*28*). These spectral characteristics and the fact that there are no Trp or disulfides to complicate the aromatic CD make the g5p and its Tyr → Phe mutants a good model system in which to examine Tyr and Phe CD contributions in our efforts to calculate protein CD (*29;* Sreerama, N., Powers, M. E., Manning, M. C., Goldenberg, D. M., and Woody, R. W., unpublished data). We have therefore undertaken a theoretical analysis of CD spectra for the newly obtained Y61F g5p and three previously studied mutants, Y26F, Y34F, and Y41F.

EXPERIMENTAL PROCEDURES

Proteins and Nucleic Acids. Wild-type g5p was isolated from *E. coli* containing a plasmid encoding the f1 g5p (*20*, *30*) or from *E. coli* 1101 *ton* 1 infected with wild-type fd virus (*5*), essentially as described by Day (*28*) with the addition of a Sephadex G75 column to remove high molecular weight contaminants (*31*). Purified g5p was quick-frozen in liquid nitrogen and stored at −80 °C. Protein contaminants were assayed using 18% polyacrylamide gels (*32*), Coomassie Blue stain, and BioPhonics Gel Print digital analysis of gel bands, yielding >98% to ≥99.5% purity. Y26F, Y34F, and Y41F g5p were derived from plasmids constructed by Terwilliger (*30*) and were isolated as above (*20*). After cell lysis with glass beads in a blender and DNAse/RNAse treatment, all of the Y61F g5p was in insoluble aggregates, and guanidine-hydrochloride solubilization and refolding by dialysis (*18*) were used to retrieve it. Y61F g5p eluted from DNA cellulose was >98% to ≥99.5% pure; Sephadex G75 chromatography was not required. Single-stranded fd DNA was isolated from fd bacteriophage, and poly[d(A)] (Sigma Chemical Co.) was prepared by serial dialyses (*20*). All nucleic acid stocks were stored frozen in 2 mM Na^+ (phosphate buffer, pH 7.0).

Spectroscopy. Measurement of UV absorption and circular dichroism, instrument calibration, calculation of extinction coefficients, and NaCl dissociation of complexes to measure binding affinities were all done as previously described (*20*). We used extinction coefficients previously given for wild-type g5p and nucleic acids, and a calculated ϵ(276 nm) of 5660 $M^{-1}cm^{-1}$ for the Tyr → Phe mutants (*20*). All spectral measurements were at 20 ± 0.5 °C. CD measurements of complexes were taken using a Jasco J710. Triple scans were run with a 10 mm path length cuvette at 50 nm/min, sensitivity 20 mdeg/cm, and response time 0.25 s. Spectral data at 0.1 nm intervals were smoothed using the Fourier smoothing routine provided by Jasco. CD spectra of nonbound proteins were taken using a Jasco 500A spectropolarimeter as described previously (*20*). To preserve fine

structure in protein CD spectra at 240−320 nm, the 1 nm data were smoothed using a 5-point quadratic-cubic function (*33*). Final CD spectra were plotted at 1 nm intervals.

CD Titrations. These were performed as previously described (*20*, *23*), measuring volumes by weighing. Aliquots of concentrated (1×10^{-4} M) g5p were added to nucleic acids, yielding complexes at final concentrations of $(4-6) \times 10^{-5}$ M in nucleotides. Precipitation during the titrations was minimal; scattering, measured as the absorption at wavelengths of ≥320 nm, was at most 5.4% relative to the absorption at 260 nm for mixtures at the highest *P*/*N* ratios.

A correction factor was applied to all plots of the CD (229 nm) to subtract the CD contribution of the nucleic acids. At wavelengths from 210 to 250 nm, the CD spectra of fd ssDNA and poly[d(A)] in complexes at $P/N = 0.25$ resemble the CD spectra of the nonbound polynucleotides at high temperatures such as 76 °C (*44*), at which temperature the magnitude of the CD is less than that at 20 °C. Therefore, the CD (229 nm, 76 °C) of the nucleic acid was subtracted from the observed 229 nm CD of the saturated complexes at $P/N \geq 0.25$. For *P*/*N* ratios between 0.0 and 0.25, the corrected 229 nm protein CD in the complex was calculated as $CD_{g5p,20^\circ} = CD_{cx,20^\circ} - [CD_{na,20^\circ} - (1/0.25)(P/N)\,(CD_{na,20^\circ} - CD_{na,76^\circ})]$, where CD_{g5p} is the corrected protein CD in the complex, CD_{cx} is the measured CD of the complex, and CD_{na} is the measured CD of the nucleic acid at the indicated temperature. CD values are calculated per mole of nucleotide. Thus, the subtracted nucleic acid CD was proportionately decreased from the value of the nucleic acid CD at 229 nm and 20 °C to the value of the nucleic acid CD at 229 nm and 76 °C, as the *P*/*N* ratio increased from 0.0 to 0.25. These corrections did not significantly change stoichiometric endpoints previously reported (*20*), but they did improve data showing a lack of 229 nm CD perturbation for the Y34F mutant (Figure 2C).

Symmetry-Corrected Association Constants. Binding constants were obtained using the simultaneous binding model of Terwilliger (*47*), which treats the g5p as a nondissociating dimer. However, we are redefining the association constant K_{int} as the symmetry-corrected intrinsic binding constant for the g5p dimer, not as the effective binding constant used in the Terwilliger model, which is twice as large due to the 2-fold rotational symmetry of the dimer. $K_{int}\omega$ values in this report are given as the product of (a) the association constant calculated using the Terwilliger model, times a symmetry factor of $^1/_2$, and (b) the ω cooperativity factor for interaction between adjacent bound dimers. The symmetry factor corrects for a 2-fold increase in the observed association constant that occurs because the 2-fold-symmetric g5p dimer can bind in two possible orientations to each available pair of sites on two antiparallel, single DNA strands. The symmetry-corrected K_{int} values directly give the free energy for binding of the g5p dimer in one orientation to the DNA. The symmetry-corrected $K_{int}\omega$ values are the same numerical values as those reported in the earlier literature for the g5p monomer, but with the revised interpretation that they are for the cooperative binding of g5p dimers.

Electron Microscopy. Electron microscopy was performed as described previously (*5*, *34*). Complexes from titrations monitored by CD spectroscopy were stabilized by cross-linking for 20 min at 20−25 °C with glutaraldehyde added to 0.08% (v/v), diluted into 0.01 M ammonium acetate (pH 6.9), and adsorbed to a carbon film made hydrophilic by exposure to a high-voltage glow discharge. The complexes were stained with 2% (w/v) aqueous uranyl acetate, dried, and imaged using Zeiss EM10CA or Philips EM400 electron microscopes. Magnifications in negatives, which were exposed after briefly maximizing lens currents to avoid magnification errors due to hysteresis, were calibrated to ±2% (combined errors) using a Fullam diffraction grating replica having 2160 lines/mm (±0.3%). Measurement of axial lengths of the complexes was done using an upgraded Numonics 1240 length calculator calibrated in our laboratory. Electron images were projected from the negatives to a total magnification of 774000×, so that the image of a complex was 60−70 cm long and the precision of the length measurements was ±2%. The separations between helical turns were most easily seen in these greatly enlarged, high-contrast negative images, and counting of turns was done by carefully tracing each helical turn in the projected images. Of the ≥100 helical turns in complexes with fd ssDNA at $n = 4$, a few turns were ambiguously delineated by the uranyl acetate stain, leading to an uncertainty of ±2−3 turns for a given complex. In the axially compressed complexes with fd ssDNA at $n = 3$ and $n \cong 2-2.5$, 5−10% of the turns were not clearly separated from their adjacent neighbors; in these regions, the number of turns was estimated as the number that would fit into the space from which stain was excluded. As indicated in Table 2, our counting methods yielded reproducible numbers for complexes at a given *n*. The absolute physical orientations of complexes tilted ±55° in the goniometer of the Zeiss EM10CA or the Philips EM400 were determined as described by Gray (*5*).

Theoretical Calculations: Rotational Strength and CD Spectra. The origin-independent matrix method (*35*, *36*) was used to compute the rotational strengths of transitions in the g5p dimer. The protein was treated as a collection of independent chromophores: the peptide groups and Tyr and Phe side chains. For the amide chromophore, $n \rightarrow \pi^*$, $\pi \rightarrow \pi^*$, $n' \rightarrow \pi^*$, and $\pi_+ \rightarrow \pi^*$ transitions were considered (*29*). For the aromatic side chains, L_a, L_b, B_a, and B_b transitions were included, using a computational model to be published elsewhere (Sreerama, N., Powers, M. E., Manning, M. C., Goldenberg, D. M., and Woody, R. W., in preparation). The energies of the transitions form the diagonal elements of the interaction energy matrix, and the electrostatic interactions between the transition moments form the off-diagonal elements. Diagonalization of this matrix gives the energies of transitions in the composite molecule, the protein dimer. The rotational strengths were then calculated for each of the excited states in the dipole-velocity formalism (*37*):

$$R_{oi} = (e^2\hbar^3/2m^2cE)(\psi_o|\nabla|\psi_i)(\psi_o|r \times \nabla|\psi_i)$$

where *E* is the energy of transition from the ground state, represented by wave function ψ_o, to the excited state, represented by ψ_i; *m* is the mass of an electron; *e* is the charge on the electron; *c* is the speed of light; and $\hbar = h/2\pi$, *h* being Planck's constant. The operators ∇ and $r \times \nabla$ are proportional to the electric and magnetic dipole transition moments in the dipole-velocity formalism.

CD spectra were calculated from the rotational strengths and the excited-state energies of the composite molecule.

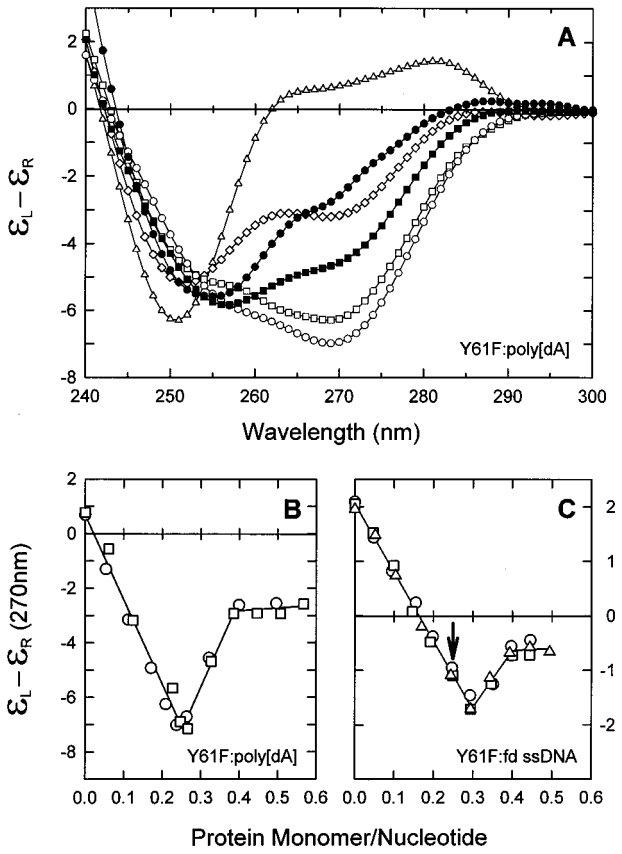

FIGURE 1: (A) Titration of poly[d(A)] with Y61F g5p, showing representative 240−300 nm CD spectra of mixtures at protein monomer/nucleotide (*P*/*N*) molar ratios of 0.0 (△), 0.11 (◇), 0.21 (□), 0.26 (○), 0.32 (■), and 0.5 (●). The filled symbols show partial reversal of the 270 nm CD at higher *P*/*N* ratios. The lower panels show plots of the CD at 270 nm as a function of *P*/*N* ratio for titration of (B) poly[d(A)] or (C) fd ssDNA with Y61F g5p. Different symbols represent data from separate titration experiments, and the solid lines are linear regressions fitted to data from all experiments. The buffer for experiments shown in all Figures was 2 mM Na^+ (phosphate, pH 7.0). The arrow in panel C indicates the single titration endpoint observed upon titration of fd ssDNA with wild-type g5p in 2 mM Na^+ (phosphate buffer, pH 7.0) plus 0.1 M NaCl (*20*). The units for $\epsilon_L - \epsilon_R$ are inverse molarity centimeters per mole of nucleotide in this and Figure 2.

Gaussian band shapes were assumed for all transitions. The relationship between the molar ellipticity and the rotational strength for the jth transition is given by

$$\Delta\epsilon_j = 2.278 R_j \lambda_j / \Delta_j$$

where $\Delta\epsilon_j$ is the maximum molar CD (M^{-1} cm^{-1}) due to transition *j*, R_j is the rotational strength in Debye−Bohr magnetons (DBM), λ_j is the wavelength of the transition, and Δ_j is the bandwidth. We assumed that the bandwidth is related to the wavelength of the transition by the following empirical relation (*38*):

$$\Delta_j = \kappa \lambda_j^{1.5}$$

where κ is a proportionality constant, which was chosen to be 0.0025, a value giving reasonable bandwidths for transitions in aromatic side chains. In earlier calculations (*29*), a larger value of κ (0.00475) was used, based upon absorption data for simple amides in solution (*39*). The bandwidth for transitions of amides in solution may be larger than that of peptide groups in proteins because of inhomogeneous broadening in solution. Empirical fitting of absorption and CD spectra of α-helical polypeptides (*40*−*42*) gives bandwidths closer to those used here.

Modeled g5p Structures. Chromophore positions needed to compute the interaction energy matrix were obtained by energy-minimizing the crystal structures of the wild-type g5p (*8*; revised PDB entry 1vqb) and the Y41F mutant (*19*; PDB entry 1yhb). Even though the crystal structures were refined at high resolution, energy minimization was performed for two reasons. First, hydrogens not explicitly included in the X-ray diffraction refinements were introduced in our calculations, using standard bond lengths and angles. Second, in most cases Tyr → Phe mutant structures were generated by deleting the phenolic oxygen of the mutated Tyr in the wild-type 1vqb structure; minimization permits the altered structure to relax. For consistency, the same minimization protocol and forcefield were applied to the original 1vqb structure before calculating CD spectra.

Two minimization protocols were followed. Protocol 1, consisting of 100 steps of steepest descent, was performed on most structures to relieve short atomic contacts with minimal changes from the crystal structure. Protocol 2 consisted of 500 steepest descents steps, 100 conjugate gradients steps, then 500 steepest descent steps to allow small rearrangements of atomic positions. We used AMBER potentials (*43*) and Biosym's InsightII 95.0/Discover 2.97 molecular modeling software. In the 1vqb structure, the missing (disordered) Arg 21 side chain was added prior to energy minimization, preserving the orientation of the C_α−C_β bond specified in the crystal structure; the missing N-terminal residue Lys 87 (disordered in the crystal) was not replaced.

RESULTS AND DISCUSSION

Y61F g5p−DNA Complexes: CD Spectroscopy

(1) Titrations: Nucleic Acid CD at 270 nm. Figure 1A shows spectra obtained during a titration of poly[d(A)] with the Y61F mutant g5p. The CD at >260 nm is due almost entirely to the nucleic acid CD, which is much greater in magnitude than is the protein CD at these wavelengths. Binding of the Y61F g5p induced dramatic nucleic acid spectral changes, similar to those induced by wild-type g5p (*23*). The nucleic acid CD at 270 nm changed from positive to increasingly negative as the protein/nucleotide (*P*/*N*) ratio was increased (Figure 1A, open symbols), followed by a partial reversal of this change at still higher *P*/*N* ratios (filled symbols). In Figure 1, panels B and C, the CD at 270 nm is plotted as a function of the *P*/*N* ratio for titrations of poly[d(A)] and fd viral ssDNA with Y61F g5p. Binding was essentially stoichiometric in 2 mM Na^+ (phosphate buffer, pH 7.0), and the titrations yielded linear plots reflecting a reduction in the 270 nm CD until a first titration endpoint was reached with one Y61F g5p monomer bound per four nucleotides of poly[d(A)] or per three nucleotides of fd ssDNA, respectively corresponding to $n = 4$ and $n = 3$ binding modes (defined in the introductory portion of this paper). Reversal of the CD change as still more protein was added led to a second titration endpoint at 1 g5p monomer per ∼2.5 nucleotides for poly[d(A)] or per 2−2.5 nucleotides for fd ssDNA. The same endpoints are found by 270 nm CD titrations with wild-type g5p (Table 1 and ref *20*).

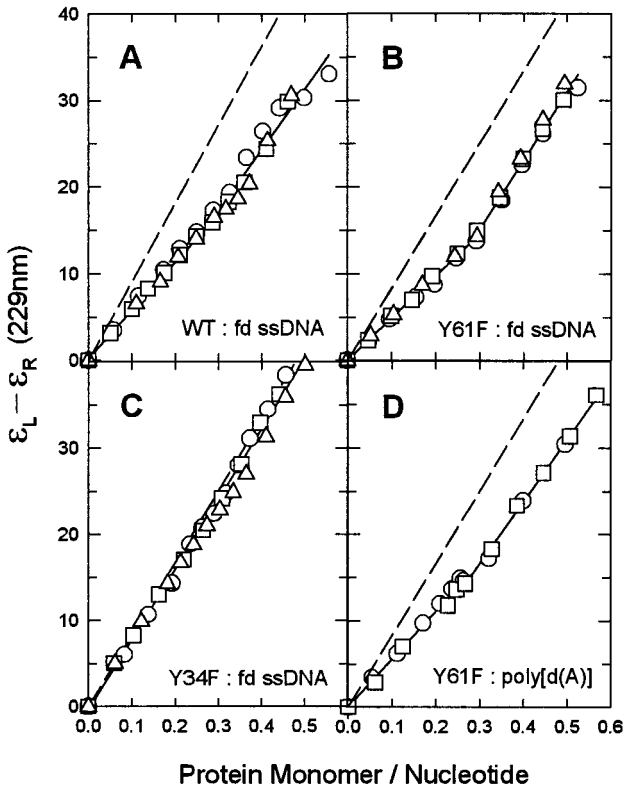

FIGURE 2: Titrations of fd ssDNA with (A) wild-type (WT), (B) Y61F or (C) Y34F g5p, and (D) titration of poly[d(A)] with Y61F g5p, monitored by changes in the protein CD at 229 nm as a function of protein monomer/nucleotide (*P*/*N*) ratio. Different symbols represent data from different titration experiments. Data were corrected for the difference in the CD of bound vs nonbound polynucleotide (see Experimental Procedures). Dashed lines represent the CD that would be observed for increasing concentrations of nonbound g5p.

Table 1: CD Titration Endpoints and Binding Modes

		P/*N* ratios at titration endpoints	
nucleic acid	binding mode[a]	wild-type	Y61F
fd ssDNA			
270 nm[b]	$n = 3$	0.35 ± 0.02	0.30 ± 0.01
	$n \cong 2-2.5$	0.46	0.40
229 nm[c]	$n \cong 3$	0.30	0.28
poly[d(A)]			
270 nm[b]	$n = 4$	0.25 ± 0.01	0.26 ± 0.01
	$n \cong 2.5$	0.39	0.38
229 nm[c]	$n \cong 3$	0.30	0.29

[a] CD-detected binding modes are expressed in terms of the site size n = the number of nucleotides occluded by each g5p monomer at endpoints in CD titrations. [b] Mean and range of values from three titrations. For $n \cong 2-2.5$ and $n = 2.5$ modes, the maximum range of values from three titrations was ± 0.05. [c] Assuming a single binding mode (see text). The 229 nm CD was corrected for nucleic acid contributions (see Experimental Procedures). For endpoints determined from two to three replicate titrations, the maximum range of the *P*/*N* ratio was ± 0.04.

In titrations monitoring g5p tyrosine fluorescence, others have found an $n = 4$ as well as an $n = 3$ binding mode for fd ssDNA titrated at low ionic strength with wild-type g5p (*26*). When fd ssDNA is titrated with wild-type g5p in 0.1 M NaCl, binding as monitored by CD does not occur in the weaker $n = 3$ mode, and a single titration endpoint (indicated by the arrow in Figure 1C) is observed at $P/N = {}^1/_4$ and $\epsilon_L - \epsilon_R = -0.8$, corresponding to the $n = 4$ binding mode (*20*). At low ionic strength, the $n = 4$ endpoint is not detected by 270 nm CD titrations of fd ssDNA with either wild-type or Y61F g5p, apparently because proteins added to the fd ssDNA when titrating from the $n = 4$ mode to the $n = 3$ mode continue to perturb the nucleic acid 270 nm CD. Taken together, these findings indicate [as was pointed out by Mark et al. (*20*)] that binding to fd ssDNA occurs in three modes, $n = 4$, $n = 3$, and $n \cong 2-2.5$.

(2) Titrations: Protein CD at 229 nm. Figure 2 shows titrations monitoring changes in the g5p tyrosyl CD at 229 nm, as a function of *P*/*N* ratio during addition of (A) wild-type, (B) Y61F or (C) Y34F g5p to fd ssDNA, or during addition of (D) Y61F g5p to poly[d(A)]. The dashed lines are the CD values calculated for additions of nonbound, unperturbed g5p to the solutions. The titration data differ in slope from the dashed lines when the 229 nm tyrosine band of g5p is perturbed by binding to the DNA.

Upon binding to fd ssDNA or to poly[d(A)], the wild-type and Y61F g5p similarly perturbed the 229 nm CD (Figure 2 and Table 1). The data of Figure 2, panels A, B, and D, could be most simply fitted by two intersecting linear regressions (shown in the figure), yielding a single endpoint at $P/N \cong {}^1/_3$ that would correspond to a single $n \cong 3$ binding mode. The second of these lines had a slope similar to that expected for additions of nonbound g5p to the titration mixture. However, these CD data would also be consistent with the existence of two g5p binding modes, $n = 4$ and $n \cong 3$, with two small changes in slope near $P/N = {}^1/_4$ (0.25) and at $P/N \cong {}^1/_3$ (0.33), as has been found when monitoring changes in g5p tyrosine fluorescence upon binding wild-type g5p to fd ssDNA and poly[d(A)] (*26*).

Wild-type g5p and three of the available Tyr → Phe mutants (Y26F, Y41F, and Y61F) exhibited a 30−42% decrease in the 229 nm molar protein CD upon binding to fd ssDNA, at the $P/N \cong 0.33$ endpoint in plots such as those of Figure 2. An exception was Y34F g5p, which failed to show perturbation of the 229 nm protein tyrosyl band upon binding to polyd[(A)] or fd ssDNA (ref *20* and Figure 2C).

(3) Protein CD Component in Complexes with poly[d(A)]. Mark and Gray (*44*) used the Y34F mutant, with its unperturbed 229 nm tyrosine band, to show that the nucleic acid CD component between 210 and 250 nm for complexes with poly[d(A)] can be largely accounted for by spectra of heated poly[d(A)], implying that poly[d(A)] in complexes with g5p is partially unstacked. Subtraction of the CD spectrum poly[d(A)] heated to 76 °C from the spectrum of Y61F g5p complexes with poly[d(A)] yielded a difference CD spectrum (Figure 1, Supporting Information) in which the 229 nm tyrosine band was substantially reduced in magnitude compared with the 229 nm CD of nonbound Y61F g5p. A similar reduction in the magnitude of the 229 nm band was previously observed for complexes with the wild-type g5p (*20*, *23*). In the case of the Y34F mutant, in which the perturbation-sensitive Tyr 34 is replaced by Phe, the difference CD spectrum was essentially identical to the CD of nonbound Y34F g5p in the 210−240 nm region, confirming the results of Figure 2C. Thus, Tyr 34 is identified as possibly the only tyrosine of the wild-type g5p that is perturbed upon binding to DNA. Also, the unchanged 210−240 nm CD of bound Y34F g5p suggests that the g5p polypeptide secondary structure is not significantly altered upon binding to poly[d(A)], consistent with information from

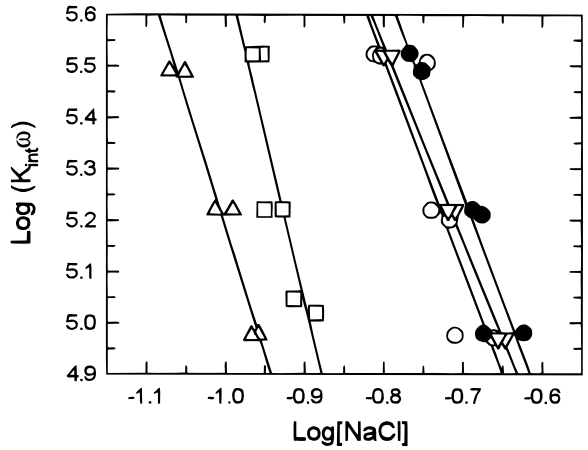

FIGURE 3: Binding affinities of wild-type (●), Y61F (▽), Y26F (○), Y34F (□), and Y41F (△) g5p for poly[d(A)], shown as plots of log($K_{int}\omega$) vs log [NaCl] for complexes formed at $P/N = {}^1/_4$ in 2 mM Na^+ (phosphate buffer, pH 7.0). Data were from duplicate dissociations of complexes at each protein concentration of 6, 12, and 21 μM. Plots of the percent change in 270 nm nucleic acid CD vs [NaCl] were used to determine the NaCl concentration that produced 50% dissociation of the complexes, i.e., 50% reversal of the maximum CD perturbation at 270 nm. $K_{int}\omega$ was determined as $1/L$, where L is the molar concentration of nonbound protein dimer at 50% dissociation (*24*, *47*), and then was corrected for dimer rotational symmetry by multiplying by a factor of $^1/_2$ (see Experimental Procedures).

Raman spectroscopy indicating that no more than a few peptide residues are perturbed by binding of wild-type g5p to poly[d(A)] (*45*).

(*4*) *Binding Affinities: Dissociation by NaCl.* A sensitive test of the functional integrity of g5p mutants is measurement of their binding affinities for polynucleotides. We define the measured binding affinity as the product of K_{int}, the symmetry-corrected intrinsic association constant for binding of a g5p dimer to a given polynucleotide, and ω, the cooperativity factor governing interactions between neighboring g5p dimers bound to the polynucleotide lattice (see Experimental Procedures). Figure 3 shows a plot of log[$K_{int}\omega$] for binding of wild-type and Tyr → Phe mutant gene 5 proteins to poly[d(A)] as a function of log [NaCl]. The values for $K_{int}\omega$ were obtained from midpoints of salt-dissociation curves for complexes formed at various total protein and polynucleotide concentrations (*20*), all at a P/N ratio of $^1/_4$. Thus, binding affinities were tested for the primary $n = 4$ mode.

The Y61F mutant had an affinity for poly[d(A)] that was only slightly less than that of the wild-type g5p. For example, values of $K_{int}\omega$ extrapolated to 0.2 M NaCl were $(1.7 \pm 0.4) \times 10^5$ M^{-1} for wild-type g5p, and $(1.4 \pm 0.1) \times 10^5$ M^{-1} for Y61F g5p. (As is explained in Experimental Procedures, these symmetry-corrected $K_{int}\omega$ values directly give the free energy for cooperative binding of a g5p *dimer* in one orientation to DNA. These values are numerically the same as those given in the earlier literature for g5p monomers, but with the corrected interpretation that these and the earlier values apply to the dimer.) The high binding affinity of Y61F g5p was in contrast to two other mutants, Y34F and Y41F, whose binding affinities were reduced by 6−30-fold in comparison with that of wild-type g5p (Figure 3 and ref *20*). The negative slopes of the lines in Figure 3, $-d(\log K_{int}\omega)/d(\log [NaCl])$, were used to estimate the number of ions released per g5p dimer during complex formation (*46*, *47*). These values were similar for wild-type (4.1 ± 0.8) and Y61F g5p (3.7 ± 0.3).

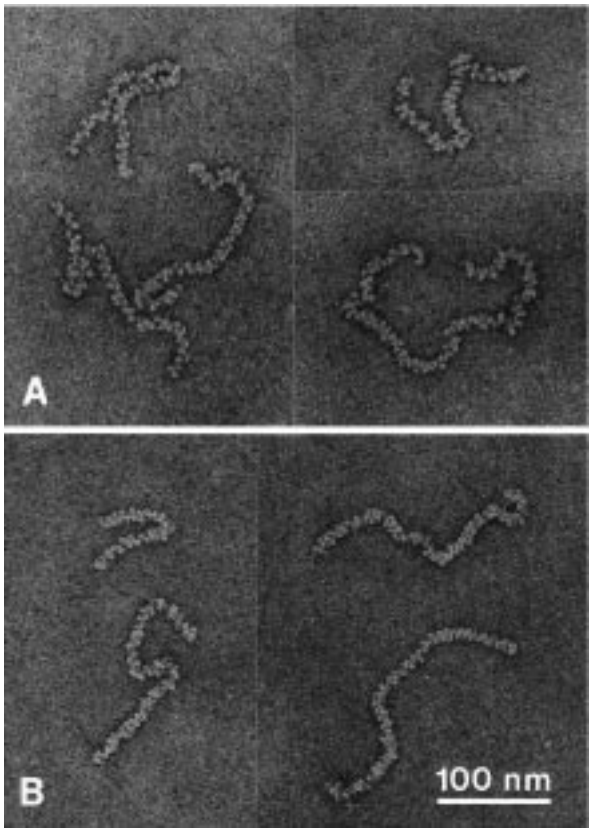

FIGURE 4: Electron micrographs of complexes of Y61F g5p with poly[d(A)] in two binding modes: (A) the $n = 4$ binding mode at a protein/nucleotide (P/N) ratio of $^1/_4$, and (B) the $n \cong 2.5$ binding mode at a P/N ratio of $^1/_2$. The $n \cong 2.5$ complexes exhibit a decreased helical pitch. Taken from CD titrations in 2 mM Na^+ (phosphate, pH 7.0) and negatively stained with uranyl acetate; scale bar = 100 nm.

A second set of salt dissociation experiments was carried out to compare the relative stabilities of the stronger and weaker Y61F g5p binding modes to increased ionic strength. Complexes were formed at a P/N ratio of $^1/_2$, with poly[d(A)] and 23 μM g5p in 2 mM Na^+ (phosphate buffer, pH 7.0), and dissociations were followed by monitoring the CD at 270 nm. The complexes with Y61F g5p were 50% dissociated from the $n \cong 2.5$ mode at 0.04 M NaCl, and from the $n = 4$ mode at a nearly 7-fold higher concentration, 0.27 M. Similarly, it has been shown (*20*) that binding of the wild-type g5p to poly[d(A)] in the $n = 4$ mode is stable to about a 10-fold higher concentration of NaCl than is binding in the $n \cong 2.5$ mode.

Y61F g5p−DNA Complexes: Electron Microscopy

(1) Changes in Structure with Binding Mode. Panels A and B of Figure 4 show complexes of poly[d(A)] titrated with Y61F g5p to a ratio of 1 g5p monomer per 4 or 2 nucleotides, respectively, corresponding to the $n = 4$ and $n \cong 2.5$ binding modes observed in titrations monitoring the CD at 270 nm (Figure 1B). The $n \cong 2.5$ complexes (Figure 4B) have a smaller helical pitch than do the $n = 4$ complexes (Figure 4A), as was shown by measuring the lengths of individual complexes of Y61F g5p with poly[d(A)] in

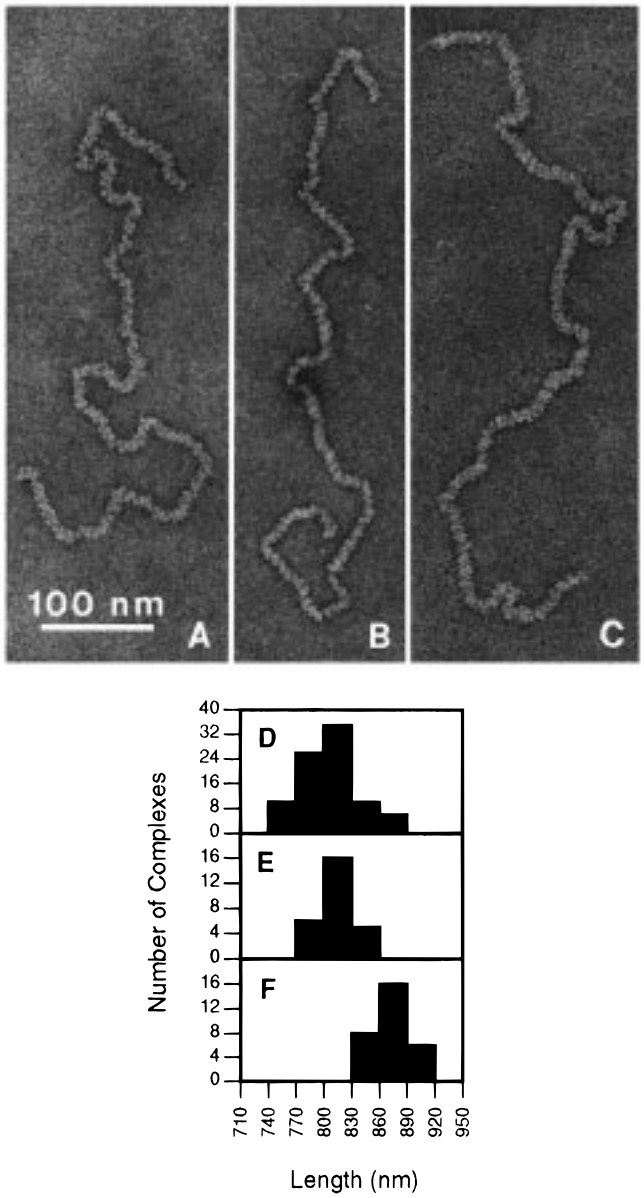

FIGURE 5: Electron micrographs of complexes of Y61F g5p with single-stranded circular fd viral DNA in three binding modes: (A), the $n = 4$ mode at $P/N = {}^1/_4$; (B), the $n = 3$ mode at $P/N = {}^1/_3$; and (C), the $n \cong 2-2.5$ mode at $P/N = {}^1/_2$. Samples were taken from CD titrations in 2 mM Na^+ (phosphate, pH 7.0) and the complexes were negatively stained with uranyl acetate; scale bar = 100 nm. The histograms show the measured lengths of populations of complexes in (D) the $n = 4$ mode, (E) the $n = 3$ mode, and (F) the $n \cong 2-2.5$ mode.

randomly selected fields and counting the turns in each complex. The measurements yielded a mean helix pitch of 7.8 ± 0.4 nm for $n = 4$ complexes, but 7.1 ± 0.2 nm for $n \cong 2.5$ complexes (Table 2).

Complexes with single-stranded circular fd viral DNA have an advantage, for studies using electron microscopy, in that the viral DNA molecules have a known length of 6408 nucleotides (*48*). Changes in contour lengths and the number of helical turns in the complexes can be quantitated as a function of changes in the mode of binding, to yield information on structural changes occurring in complexes with this DNA substrate of constant length. Panels A, B, and C of Figure 5 show complexes of Y61F g5p with individual molecules of fd ssDNA, at *P*/*N* ratios of 1 g5p monomer per 4, 3, or 2 nucleotides, respectively. These complexes correspond to binding of the Y61F g5p in the $n = 4$, $n = 3$, or $n \cong 2-2.5$ modes described in the preceding sections. In each of these complexes, two equal segments of the circular single-stranded viral DNA run in opposite directions along the length of the flexible nucleoprotein helix, held in place by interactions with oppositely oriented DNA binding sites on the g5p dimers (*5*).

The population of $n = 4$ complexes of fd ssDNA with Y61F g5p (Figure 5A) appeared to be saturated with protein, judged by the uniform lengths of the complexes (Table 2) and a lack of visible single-stranded DNA segments. This was previously found to be the case for $n = 4$ complexes with wild-type g5p (*6, 49*), consistent with the observation of an $n = 4$ binding mode for wild-type g5p at low ionic strength by fluorescence titrations (*26*).

Table 2 summarizes the differences in the helical structures of the complexes represented in Figure 5. As the *P*/*N* ratio increases from ${}^1/_4$ to ${}^1/_3$ to ${}^1/_2$ and the binding mode changes from $n = 4$ to $n = 3$ to $n \cong 2-2.5$, the mean number of turns in these complexes (all containing fd ssDNA of the same length) increases from (104 ± 3) to ($\sim 113 \pm 3$) to ($\sim 123 \pm 3$). (The number of turns in $n = 3$ and $n \cong 2-2.5$ complexes was estimated as described in Experimental Procedures.) The mean contour length of the complexes increases from 820 ± 30 to 890 ± 20 nm, as is shown in Table 2 and in histograms D−F of Figure 5, and at the same time, the mean helix pitch decreases from 7.9 ± 0.2 to 7.3 ± 0.1 nm. Thus, as binding progresses from the $n = 4$ to the $n = 3$ to the $n \cong 2-2.5$ mode, the binding of additional g5p dimers to fd ssDNA is accompanied by increases in the number of helical turns and in the contour lengths of the complexes. There is a concomitant decrease in the mean helix pitch, presumably reflecting a compression of the helical structure as an increased number of bound proteins and added helical turns are accommodated on the DNA.

(2) Structure of Y61F versus Wild-Type g5p Complexes. The Y61F g5p complexes of Figures 4 and 5 and Table 2 are indistinguishable, at the level of structural resolution afforded by electron microscopy, from the corresponding complexes formed with wild-type g5p (*5, 6*). Both the wild-type and Y61F g5p nucleoprotein superhelices are highly flexible, particularly at a *P*/*N* ratio of ${}^1/_4$ (Figures 4A and 5A), and the local helix pitch varies somewhat to accommodate axial curvature. The nucleoprotein superhelices formed by Y61F g5p with poly[d(A)] and fd ssDNA were shown to be left-handed, by tilting the complexes ±55° about an axis perpendicular to the helix axis as previously described (*5, 34*). A left-handed helical sense was previously demonstrated (*5, 6*) for superhelices formed by the wild-type g5p with fd ssDNA, poly[d(A)], and poly[r(A)]. Wild-type g5p complexes with fd ssDNA contain 103 ± 3 helical turns at $P/N \cong {}^1/_4$ (*6*), indistinguishable from the 104 ± 3 turns found for Y61F g5p complexes at $P/N = {}^1/_4$ (Table 2). The complexes with wild-type and Y61F g5p show similar increases in the number of helical turns and decreases in the mean helix pitch at increased *P*/*N* ratios. The measured widths of complexes with Y61F g5p are similar to those of wild-type complexes, which were estimated to have a diameter 8 ± 1 nm, after tilting 0° and 55° about the helix axis to obtain an approximate correction for flattening (*5, 6*).

Table 2: Measurements from Electron Microscopy of Complexes with Y61F g5p[a]

nucleic acid	*P*/*N* ratio[b]	binding mode	mean helix pitch (nm)[c]	mean complex length (nm)[d]	mean number of helical turns[e]	g5p dimers per turn[f]
fd ssDNA	$^1/_4$	$n = 4$	7.9 ± 0.2	820 ± 30	104 ± 3	7.7 ± 0.3
	$^1/_3$	$n = 3$	7.3 ± 0.2	820 ± 20	∼113 ± 3	9.5 ± 0.3
	$^1/_2$	$n \cong 2-2.5$	7.3 ± 0.1	890 ± 20	∼123 ± 3	∼10−13
poly[d(A)]	$^1/_4$	$n = 4$	7.8 ± 0.4	190 (48−285)	26 (7−32)	
	$^1/_2$	$n \cong 2.5$	7.1 ± 0.2	226 (91−291)	33 (14−40)	

[a] Measured on complexes taken from CD titrations in 2 mM Na^+(phosphate buffer, pH 7.0). [b] Molar ratio of protein monomers to nucleotides. [c] Based on measurements of the length and number of turns in clearly defined helical segments; at least 100 turns were averaged for each species. Values are reported as ± 1 sd. [d] Based on measurement of contour lengths of 87, 27, 30, 23, and 18 complexes, progressing down the table from complexes with fd ssDNA at $P/N = {}^1/_4$. Reported as mean ± 1 sd.; numbers in parentheses are ranges of measured lengths, for complexes with polynucleotides that are heterogeneous in length. [e] Counted in 16, 6, and 6 $n = 4$, $n = 3$, and $n \cong 2-2.5$ complexes with fd ssDNA, and in the same poly[d(A)] complexes as in footnote *d*. The number of turns in $n = 3$ and $n \cong 2-2.5$ complexes with fd ssDNA was estimated as described in Experimental Procedures. Reported as mean ± the range of observed values, or as mean with a range in parentheses. [f] Calculated for complexes with the 6408 nucleotide fd ssDNA as 6408/(2*nt*), where *t* is the mean number of turns per complex at a given *P*/*N* ratio and *n* is the number of nucleotides per bound g5p monomer, assumed to be 4, 3, and 2.5−2 at *P*/*N* ratios of $^1/_4$, $^1/_3$, and $^1/_2$, respectively.

Conclusions: Y61F g5p and Its Complexes

(1) Y61F g5p Aggregates during Expression but Functions Normally after Refolding. All of the Y61F g5p in plasmid-transformed *E. coli* was insoluble (unlike plasmid-encoded wild-type g5p) and could only be recovered after solubilization with 6 M guanidine hydrochloride, followed by refolding during dialysis at 4 °C to remove the guanidine. Yet, the refolded Y61F g5p appears to be functionally similar to the wild-type g5p. The Y61F and wild-type gene 5 proteins exhibit the same set of multiple binding modes in CD binding titrations, and the binding affinity of Y61F g5p is only slightly reduced from that of wild-type g5p. Complexes formed between Y61F g5p and ssDNAs display the same perturbations of protein and nucleic acid CD bands that occur for complexes formed with wild-type g5p. Electron microscopy provides a strong confirmation that the Y61F g5p is structurally normal, showing that the Y61F g5p forms the same helical structures as does the wild-type g5p. The Tyr → Phe replacement has little effect on the interactive functions residing on the surface of this small protein: formation of protein dimers, binding of the dimers to single-stranded polynucleotides, and cooperative dimer−dimer interactions to form the nucleoprotein superhelix that is visualized by electron microscopy.

These findings suggest that the Y61F g5p may fail to fold properly after its expression in bacterial cells, like the temperature-sensitive folding mutants described by King and colleagues (*50, 51*), and like many unstable variants of g5p (*18, 22, 52*). Tyr 61 may be a sensitive locus on the g5p, since there are reports of aggregation and reduced biological activity for two other Tyr-61-substituted g5p mutants, Y61H and Y61S (*18, 22*). Unlike one group of folding mutants of phage P22, in which mutations occur at the protein surface in turns of the polypeptide chain (*51*), the Y61F substitution occurs in a buried residue in the middle of a strand of the g5p β-sheet structure. This substitution does not introduce bulk, but it would eliminate the hydrogen bonds found between the Tyr 61 hydroxyl and the peptide N and O of Ala 57 in the crystal structure of the wild-type g5p (*19*). Apparently, these hydrogen bonds are not critical for stabilization of the native protein structure, at least under the conditions we used for study of the refolded Y61F g5p in vitro. Hydrogen bonds formed with the Tyr 61 hydroxyl might help to prevent unfolding under more stringent conditions, or they might help to control the folding process in vivo. Close interaction of the Tyr 56 and Tyr 61 (or Phe 61) aromatic rings as described by Burley and Petsko (*53*) may help to stabilize the folded protein structure, even in the absence of the Tyr 61 hydroxyl.

(2) Polynucleotide Release in Secondary Binding Mode. The initial change in the 270 nm CD of poly[d(A)] during titrations with g5p may be due to induced alterations of the DNA winding angle, as in dehydration of double-stranded DNA (*54*), or to a substantial negative tilt of the bases (*55*). At low ionic strength, there is a partial restoration of the nucleic acid CD at 270 nm when poly[d(A)] is further titrated from the first endpoint at $n = 4$ to the second endpoint at $n \cong 2.5$. This reversal suggests that there may be a partial release of the poly[d(A)] bases (which have a strong tendency to stack with one another) from interaction with each bound g5p (*20*).

Fluorescence titrations at low ionic strength show distinct $n = 4$ and $n = 3$ binding modes for the binding of g5p to fd ssDNA as well as to poly[d(A)] (*26*). However, the first apparent endpoint in 270 nm CD titrations of fd ssDNA with g5p is at $n = 3$, apparently because the changeover from the $n = 4$ to the $n = 3$ mode is not accompanied by a detectable change in the perturbation of the 270 nm polynucleotide CD that is induced by each molecule of bound g5p. The fd ssDNA contains thymine residues, for which the wild-type g5p is known to have an extremely high affinity (*56, 57*), and fd ssDNA binds to g5p with substantially higher affinity than does poly[d(A)] (*25*). The greater affinity of the g5p for the nucleotides of fd ssDNA may prevent a partial release of the nucleotides in going from the $n = 4$ to the $n = 3$ mode. The 270 nm CD data indicate that binding of g5p to fd ssDNA at low ionic strength can progress still further, to saturate the DNA in a third binding mode in which each g5p interacts with still fewer nucleotides ($n \cong 2-2.5$). In this third mode, there is a partial recovery of the CD at 270 nm, also possibly due to partial release of the nucleotides from each bound g5p.

(3) Role of Tyr 34 in Binding. Upon binding to fd ssDNA or poly[d(A)], the 229 nm tyrosyl CD is substantially decreased in the wild-type g5p and in all Tyr → Phe g5p mutants tested except Y34F (Figure 2C and ref *20*). This implies that Tyr 34 is involved in interactions that affect the 229 nm tyrosyl CD band. The Tyr 34 residue is partially exposed at the protein surface and is only 10 Å distant from Tyr 41, which has been implicated in dimer−dimer coopera-

tive interactions (see introductory portion of this paper). An effect of cooperative interactions on Tyr 34 may be involved in the perturbation of the 229 nm CD (*20*). Notably, a reduced CD perturbation at 229 nm occurs upon binding of the wild-type g5p to the DNA oligomers $d(pA_7)$ and $d(pA_{20})$, whose short lengths preclude extensive cooperative interactions (*23*).

(4) The Superhelix Structure Changes with Binding Mode. Figure 5 shows complexes formed by the Y61F g5p with fd ssDNA in the $n = 4$ (A), $n = 3$ (B), and $n = 2-2.5$ (C) binding modes. Complexes in the latter two modes have a reduced helix pitch and/or an increased length compared with complexes in the $n = 4$ mode (Figure 5 and Table 2). Similar changes are seen in the corresponding complexes of wild-type g5p with fd ssDNA (*6, 49*).

The structural changes found by electron microscopy for Y61F g5p complexes with fd ssDNA correspond to an increasing number of g5p dimers per helical turn, from (7.7 ± 0.3) to (9.5 ± 0.3) to ($\sim 10-13$) for the $n = 4$, $n = 3$, and $n = 2-2.5$ modes, respectively (Table 2). Dividing the 6408 nucleotides of fd ssDNA by the number of helical turns yields an estimated 62, 56, and 52 nucleotides of ssDNA per turn in the $n = 4$, $n = 3$, and $n = 2-2.5$ modes, or about 31, 28, and 26 DNA nucleotides in each of the two single-stranded DNA segments that traverse a helical turn, running in opposite directions. These findings clearly demonstrate that g5p dimers are not added to $n = 4$ complexes by simply adding superhelical turns having the same structure as do helical turns at $n = 4$. If this were the case, $n = 3$ complexes would be predicted to have $^4/_3 \times 104 = 139$ helical turns, a number that is dramatically different from our estimate of $\sim 113 \pm 3$ turns (Table 2). Electron microscopy thus shows that transitions among the three binding modes involve changes in the fundamental structural arrangement of proteins and DNA in each turn of the nucleoprotein superhelix, resulting in an *increase* in the number of g5p dimers, but a *decrease* in the number of DNA nucleotides, associated with each helical turn.

Four Tyr → Phe g5p Mutants: Analysis of CD Spectra

(1) Tyrosine Locations and Mobilities. The five tyrosines of the wild-type g5p occur in three groups: the Tyr 56/Tyr 61 pair in the protein core, Tyr 34 and nearby Tyr 41 on the presumed dimer-dimer interface, and Tyr 26 on the extended DNA-binding loop. The relative mobilities of the tyrosyl rings were estimated by adding hydrogens to all residues and then rotating about the Tyr $C_\beta-C_\gamma$ bond, checking for van der Waals overlaps amounting to $\geq 10\%$ of the sum of the radii of contacting atoms of the Tyr and neighboring residues. The Tyr 56/Tyr 61 pair is largely buried in the hydrophobic protein interior, with only the tyrosyl hydroxyls exposed to solvent. The two rings interact at a dihedral angle of 66°, with the ring centers separated by only 5−6 Å. By our approximate test of rotational mobility, Tyr 56 or Tyr 61 can rotate through arcs of ∼30 or 45° (of a possible 180°). Tyr 41 projects outward from the protein surface, with its ring fully exposed to solvent; the ring can rotate ∼100° about the $C_\beta-C_\gamma$ bond, if there is concomitant rotation about $C_\alpha-C_\beta$ to avoid contacts with nearby residues. Tyr 34 is partially embedded in the protein surface, with ∼65° of rotational freedom about $C_\beta-C_\gamma$. Tyr 26 is on an extended polypeptide loop, but its rotation about $C_\beta-C_\gamma$ is limited to ∼45° due to extensive contact of one side of the tyrosyl ring with the backbone structure of the loop.

(2) Protein CD of Wild-Type g5p and Tyr → Phe Mutants: 250−300 nm. Figure 6 compares the CD spectra of wild-type g5p and Y26F, Y34F, Y41F, and Y61F mutants. In this long-wavelength aromatic region where tyrosyl and phenylalanyl L_b bands dominate, the spectra of Y61F and Y34F g5p differ markedly from one another and from the wild-type spectrum. Phenylalanine lacks CD bands above 270 nm (*58, 59*). If the structures of the wild-type and mutant proteins are similar except for the Tyr → Phe substitution and if the spectral contributions are additive, then Tyr 34 and Tyr 61 must make negative contributions to the wild-type g5p spectrum at 250−290 nm and 255−280 nm, respectively, since replacement of these Tyr by Phe leads to large positive Tyr CD bands in these regions.

The negative Tyr 34 and Tyr 61 CD contributions are shown in the CD difference spectra of Figure 7A, in which the measured CD of each mutant is subtracted from the CD of wild-type g5p. CD difference spectra above 270 nm reveal the CD bands contributed by the Tyr that was replaced by a Phe. Both Tyr 34 and Tyr 61 make substantial negative contributions to the wild-type CD above 270 nm, whereas Tyr 26 and Tyr 41 make relatively small positive contributions in this region. Tyr 56, for which no Phe substitution mutant is available, apparently contributes (or induces) a strong positive CD in this region, compensating for the negative CD contributions of Tyr 34 and Tyr 61 in the CD spectrum of the wild-type protein.

There is an unusual negative band at 286−288 nm (Figure 6A) in the spectra of all g5p except the Y34F mutant. As is discussed in Supporting Information, this may be a residual tail of the strong negative 284 nm band of Tyr 34.

(3) Phe 34 and 61 are in Well-Defined Environments. Each of the four Tyr → Phe g5p mutants has a unique CD spectrum at long wavelengths (Figure 6A), confirming that these four Tyr reside in different environments in the g5p structure. The Y34F and Y61F spectra in Figure 6A exhibit marked Phe fine structure, with minima in the 249−269 nm region (corresponding to maxima in Figure 7A) that are separated by 6.3−6.5 nm and represent the vibronic components of a negative Phe L_b band (*58, 60*). Less dramatic but still distinct are minima due to the replacement Phe in the Y26F difference spectrum of Figure 7A. This suggests that all three Phe side chains are in well-defined chemical environments that do not change substantially due to movement of neighboring residues or reorientation of the Phe rings. Furthermore, the L_b bands of the Tyr and replacement Phe have the same sign in all three cases, suggesting similar ring orientations. These features are consistent with the fact that these residues all have limited mobility as described above.

(4) Protein CD of Wild-Type g5p and Tyr → Phe mutants: 180−250 nm. Figure 6B shows CD spectra of the wild-type g5p (filled circles) and the Tyr → Phe mutants. CD spectra in the 180−250 nm region generally reflect protein secondary structure, and β-sheet polypeptides usually exhibit a broad negative band near 217 nm (*61*). Although the g5p is predominantly a β-structure (*8*), the 210−250 nm CD of the wild-type and Tyr → Phe mutant gene 5 proteins

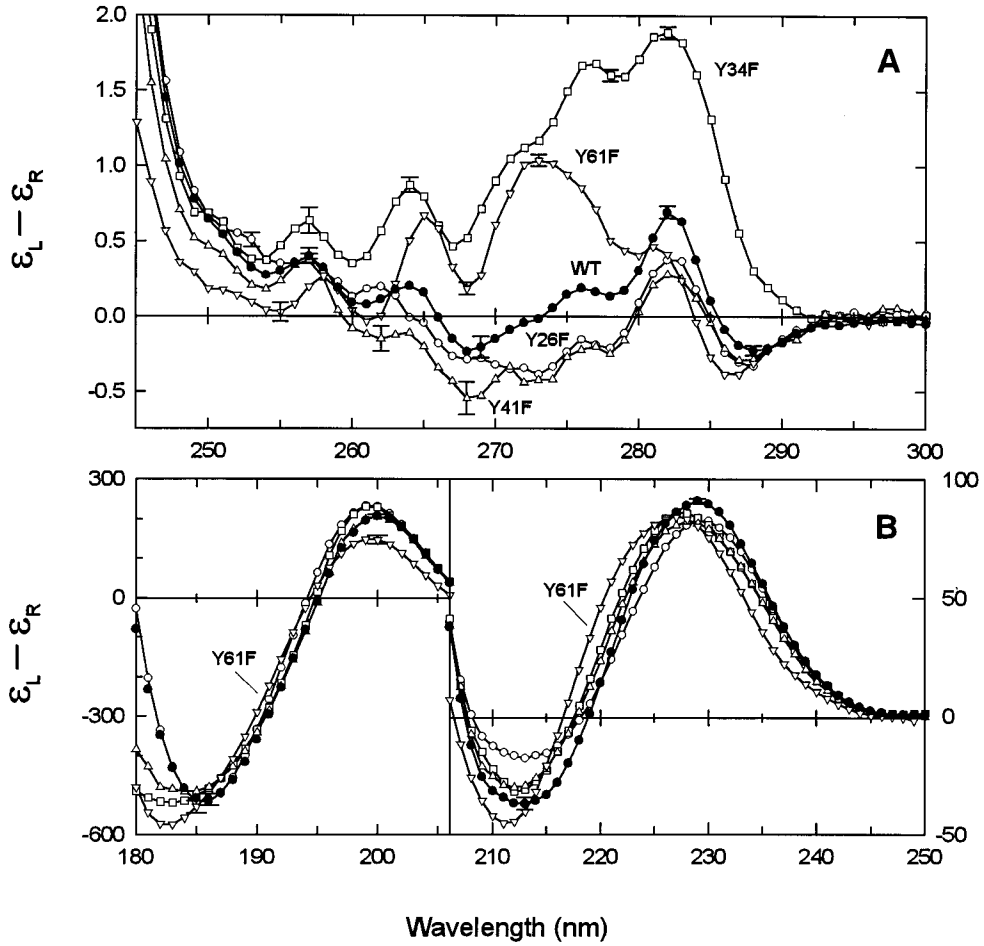

FIGURE 6: CD spectra of wild-type and mutant gene 5 proteins, (A) at 245−300 nm (near-UV), and (B) at 180−250 nm (far-UV). The symbols represent wild-type (●), Y26F (○), Y34F (□), Y41F (△), and Y61F (▽) g5p. Error bars show the range of values from three spectral measurements. In panel B, error bars are drawn for Y61F g5p at 185 and 200 nm, and for wild-type g5p at 186, 200, 213, and 229 nm; at some wavelengths the error bars are as small as the symbols and are barely visible. The units for $\epsilon_L - \epsilon_R$ are inverse molarity centimeters per mole of g5p monomer in this and Figures 7 and 8.

is dominated by a large, positive 229 nm band attributable to the Tyr L_a band, as was first noted by Day (*28*). The 229 nm band of wild-type g5p is decreased by <10% in each of the four available Tyr → Phe mutants, suggesting that Tyr 56, the only g5p Tyr that has not been experimentally replaced by Phe, may dominate the L_a band as well as having a large L_b band.

(5) Evidence for Native Structure of g5p Mutants. The retention of the 229 nm band in all of the g5p mutants (Figure 6B) suggests that the mutant gene 5 proteins retain the native OB-fold structure, since this band disappears upon denaturation of the g5p (*62*). Supporting this conclusion is the fact that all of the mutants have nearly normal binding stoichiometries and the Y26F and Y61F proteins have essentially normal DNA binding affinities and form complexes having normal structures (ref *20*, this communication, and C. W. Gray, unpublished data). The Y41F mutant, which binds the most weakly, has been shown to have a crystal structure that is almost indistinguishable from the wild-type structure (*19*).

(6) Calculated Protein CD Difference Spectra. The calculated absolute CD spectra (*not shown*) differ substantially from the experimental spectra. (As is noted below, the reasons for this appear to lie in our treatment of the peptide transitions and affect mainly the short wavelength CD.) We therefore compare experimental and theoretical CD difference spectra in Figure 8. Except where otherwise specified, theoretical difference spectra were calculated using the wild-type g5p structure and computer-derived mutant g5p structures, energy-minimized using protocol 1. Comparisons between experimental and theoretical CD difference spectra are presented in two wavelength regions: (1) the near-UV (250−300 nm), where the contributions from peptides are negligible and the CD difference spectra correspond primarily to the L_b transition of Tyr, and (2) the far-UV (205−250 nm), where the contributions from peptides are mixed with those of the L_a transitions of Tyr and Phe. Vibronic fine structure, evident in the experimental difference spectra of Figures 7A and 8, is not taken into account in the calculated spectra.

For the Y26F and Y34F mutants, good qualitative agreement was obtained between theory and experiment in the near-UV. Theoretical CD difference spectra predict a positive couplet for the Y26F g5p and a very asymmetric negative couplet with a dominant negative lobe for the Y34F g5p. The presence of vibronic fine structure in the experimental CD difference spectra, together with an exaggeration of magnitude in the theoretical spectra, tends to obscure the qualitative agreement between theory and experiment. In the theoretical difference spectra, the short-wavelength lobe due to the replacement Phe is a single broad band, whereas in the experimental spectra, the Phe contribution is distributed

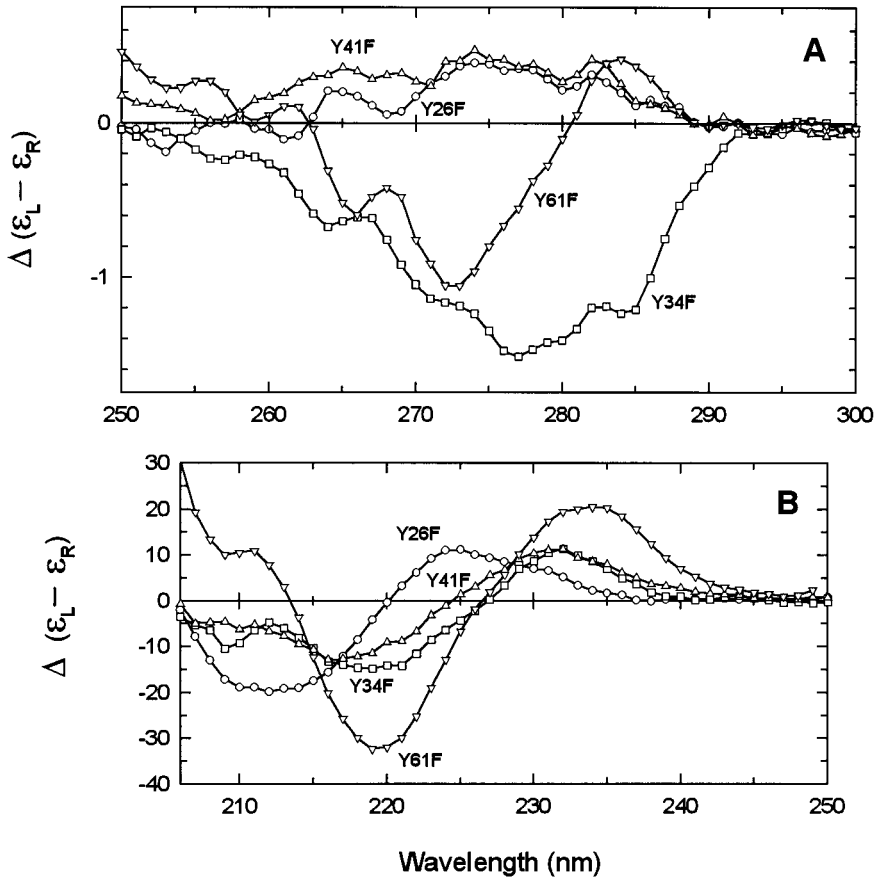

FIGURE 7: Difference CD spectra of wild-type minus mutant gene 5 proteins, from the spectra of Figure 6, (A) at 250−300 nm and (B) at 205−250 nm. The symbols represent the CD of wild-type g5p minus the CD of Y26F (○), Y34F (□), Y41F (△), or Y61F (▽) g5p.

among sharp bands superimposed on the broader Tyr contribution of opposite sign.

For the Y41F g5p, the two theoretical near-UV CD difference spectra correspond to two structures used for calculations: first, the mutant structure obtained by deleting the tyrosyl oxygen of Tyr 41 of the 1vqb wild-type g5p crystal structure (*8*) and, second, the Y41F 1yhb crystal structure of Guan et al. (*19*). Both calculated difference spectra predict negative bands near 280 nm, in disagreement with the positive band found in the experimental spectrum.

For Y61F g5p, the experimental near-UV CD difference spectrum consists of a positive couplet with substructure in the shorter wavelength negative band. Two theoretical CD difference spectra are shown for Y61F g5p, corresponding to two protocols used to minimize the Tyr → Phe substituted structure; both have a positive band near 280 nm. The theoretical CD difference spectrum obtained using minimization protocol 2 gives better agreement with experiment, with a positive couplet in contrast to the single positive feature predicted for the structure minimized using protocol 1. In the best case, there is still an overestimate of the magnitude, and the crossover is shifted to a shorter wavelength relative to the experimental difference spectrum. For the Y56F g5p, the predicted CD difference spectrum has a negative band in the near-UV, with a larger amplitude predicted for the structure minimized using protocol 2. However, the sign of this predicted Y56F band does not agree with the sign inferred from the measured spectra of other mutants (see subsection 2 above).

As was the case in the near-UV, experiment and theory agree best in the far-UV for the mutants Y26F and Y34F, for which theory predicts the observed positive couplets centered near 225 nm, but with a substantial shift to longer wavelengths relative to the experimental data for the Y26F g5p. For the Y41F mutant, the experimentally observed positive couplet in the far-UV is not predicted; neither calculation gives a qualitatively correct prediction. For Y61F g5p, minimization using protocol 2 gives better results than protocol 1 in the near-UV but poorer results in the far-UV. For Y56F g5p, both calculations predict a positive couplet in the far-UV.

(7) Calculated CD Spectra: Limited Mobility of Residues 26 and 34. Overall, the calculated and experimental difference CD spectra give the best agreement for the mutants Y26F and Y34F. The calculated difference spectra for these mutants are qualitatively correct in both the near- and far-UV, although the magnitudes are considerably overestimated in the near-UV and somewhat underestimated in the far-UV. The theoretical spectra correspond to a single geometry, a minimum energy configuration, for each of the proteins, whereas the experimental spectra correspond to an average over an ensemble of conformations in solution. Although they are exposed at the protein surface in the g5p crystal structure, Tyr 26 and Tyr 34 have limited torsional mobility. Good qualitative agreement between theory and experiment suggests that the wild-type, Y26F, and Y34F structures used to calculate the CD approximately represent the average structure in solution.

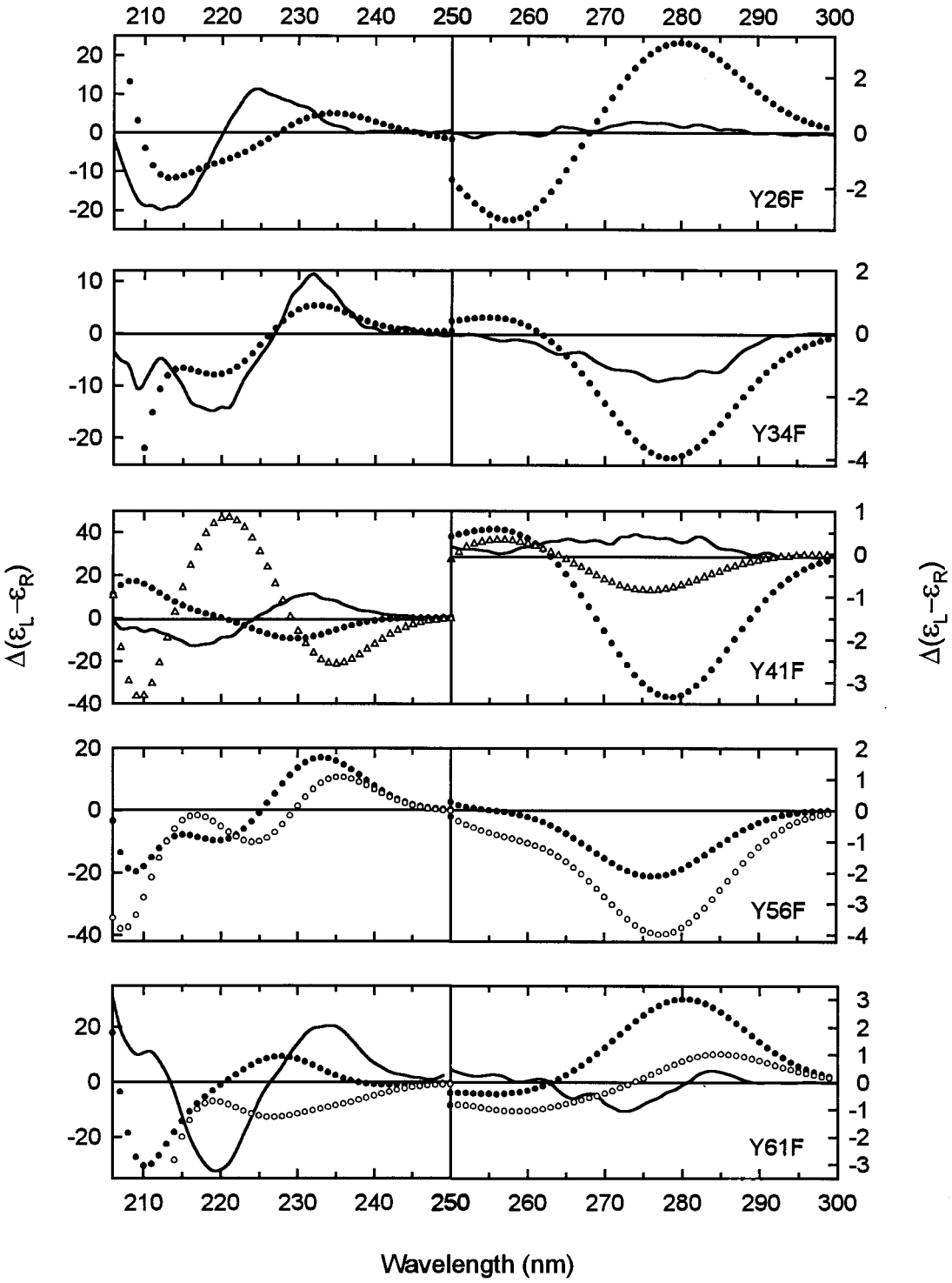

FIGURE 8: Difference CD spectra of wild-type and Y34F g5p, comparing measured (—) and theoretically calculated (●, △, ○) spectra at 205−250 nm (far-UV) and at 250−300 nm (near-UV). Note that the difference CD scales differ in these two wavelength ranges and in the plots for various Tyr → Phe mutants. The calculated spectra are based on g5p crystal structures subjected to computer-simulated mutation and energy minimization protocols described in Experimental Procedures. For those calculated spectra that are shown as (●), the wild-type g5p structure was minimized using protocol 1, mutated, and again minimized using protocol 1. For Y41F, (△) is a calculated spectrum based on the crystal structure of the Y41F g5p mutant; this structure was minimized using protocol 1. For Y56F and Y61F, (○) is a calculated spectrum obtained after minimizing the wild-type crystal structure using protocol 1, mutating, and more extensively minimizing the mutated structure using protocol 2. No Y56F mutant was available to provide an experimental CD spectrum.

(8) Calculated CD Spectra: Tyr 41 Orientation in Solution vs Crystal. In both the near- and far-UV spectral regions, theory gives poor agreement with experiment for Y41F g5p. Using the Y41F crystal structure as the starting point, rather than the wild-type crystal structure, gives somewhat improved results in the near-UV but poorer agreement in the far-UV. The relatively high torsional mobility of Tyr 41 about the $C_\beta-C_\gamma$ bond is probably responsible for the failure of theory to predict qualitatively correct difference spectra for the Y41F mutant. The CD of Tyr 41 in solution may be dominated by rotamers quite different from the rotamer that is stabilized in the crystal. The L_b bands of Tyr and Phe,

which dominate the near-UV spectra, are especially sensitive to torsion about the $C_\beta-C_\gamma$ bond because the L_b transition moment is perpendicular to this bond and thus rotates as the dihedral angle χ_2 varies. (In contrast to this, the L_a transition moment is polarized along the $C_\beta-C_\gamma$ bond direction, and therefore its direction is invariant with respect to torsion about the $C_\beta-C_\gamma$ bond. The L_a transition, however, mixes with the peptide $n \rightarrow \pi^*$ transition, making the L_a band more sensitive to the relative orientations of the aromatic side chain and peptide groups in the wild-type and mutant g5p.)

(9) Calculated Spectra: Tyr 61 and Sensitivity of CD Spectra to Small Structural Changes. The largely buried Tyr 61 residue has limited potential mobility in the g5p crystal structure, and it should have strong optical interactions with the adjacent, largely buried Tyr 56, from which it is separated by only 5−6 Å. Tyr 61 should also interact to a lesser extent with Tyr 34, which is 13−15 Å distant from the Tyr 56/Tyr 61 pair. Small changes in the relative orientations and local environments of these tyrosines could have a large effect on the CD. This may account for the fact that the calculated difference CD of the Y61F mutant shows rather poor agreement with experiment.

Our present study reveals a high degree of sensitivity of the calculated CD to the structures used for calculation. This is exemplified by the significant differences in rotational strengths (section 10 below) and calculated CD difference spectra (Figure 8) that result when the Y41F g5p crystal structure is used instead of a computer-mutated wild-type crystal structure, or when a more extensive energy minimization protocol is applied to computer-mutated wild-type crystal structures. The wild-type vs Y41F crystal structures are very similar, with an rmsd for all atoms of 0.91 Å (*19*). It appears that the calculated CD may be dependent on structural details that are finer than those determined by X-ray crystallography. Comparison of the positions of all heavy atoms in our Y56F structures energy minimized by protocol 1 vs protocol 2 yields an rmsd of only 0.54 Å; the corresponding rmsd for our Y61F structures after minimization by protocols 1 vs 2 is 0.56 Å. These small changes lead to significantly different calculated CD difference spectra (Figure 8, open vs filled circles for Y56F and Y61F), again indicating that the calculated difference CD is sensitive to very small structural changes.

A better approach to generate mutant structures approximating average solution structures may be the use of restrained molecular dynamics, allowing for CD calculations based on a range of local conformations occurring in the vicinity of the mutated residue. Koslowski et al. (*63*) obtained improved results for pancreatic ribonuclease upon averaging over an in vacuo molecular dynamics trajectory. Further improvements should be obtained by including solvent in the simulation that is used as a basis for the CD calculations.

(10) Calculated Rotational Strengths. The theoretically calculated rotational strengths for the Tyr L_b and L_a bands are given in three tables in the Supporting Information. On an energy scale, the L_b bands are sufficiently distant from other transitions that mixing with such transitions is relatively weak. In the g5p dimer, a given pair of equivalent tyrosines (for example, the Tyr 26 side chains on two monomers) gives rise to two transitions that are predominantly in-phase and out-of-phase combinations of the L_b transitions of this tyrosine on the two monomers, and the net rotational strength from these transitions can be attributed to this pair of tyrosines. The strongly coupled tyrosines Tyr 56/Tyr 61 give rise to four transitions in the dimer. In the g5p mutants, the L_b transition of the mutated side chain is that of a Phe, rather than a Tyr, and occurs near 260 nm rather than near 280 nm. The L_b rotational strength for the Phe side chain that replaces a Tyr generally has the same sign as that of the Tyr for which it substitutes.

As was noted in subsection 2 above, the experimental spectra of Figure 7 show that the L_b rotational strengths of Tyr 26, Tyr 34, Tyr 41, and Tyr 61 are, respectively, small and positive, large and negative, small and positive, and large and negative. By inference, Tyr 56 has a large positive L_b rotational strength. The calculated rotational strengths are in qualitative agreement with experiment for Tyr 26 and Tyr 34, but the prediction for Tyr 41 is incorrect in sign. The rotational strengths are not inconsistent with the combination of Tyr 56 and Tyr 61. For the three Tyr side chains that are not strongly coupled, the calculated L_b rotational strengths generally do not show large variations between the wild-type and the mutants, supporting the assumption of additivity that was made in interpreting the CD difference spectra of Figure 7 as being due to spectral contributions of the individual Tyr that were replaced by Phe.

Analysis of the L_a rotational strengths is much more complex because the L_a transitions mix strongly among themselves and with the peptide backbone $n \rightarrow \pi^*$ transitions. Some peptide $n \rightarrow \pi^*$ transitions are shifted from their normal wavelength near 220 nm to about 230 nm, so that they are approximately degenerate with the Tyr L_a bands. This results from strong static-field mixing of the peptide $n \rightarrow \pi^*$ and the lowest energy $\pi \rightarrow \pi^*$ transitions. Because of the strong negative rotational strength predicted theoretically for the region of the L_a band, the absolute spectra calculated from theory fail to show the observed strong positive feature in the 230 nm region. However, the difference between the wild-type and mutant g5p is predicted qualitatively correctly, in most cases. The largest positive value is predicted for the Y56F g5p, which is also inferred to be the case from the experimental data. The one case for which the difference in rotational strengths disagrees in sign with the observed difference spectrum near 230 nm is Y41F g5p, for which a negative difference is predicted, in contrast to the observed 230 nm difference CD. This discrepancy is substantially magnified if the Y41F crystal structure is used, rather than the wild-type crystal structure.

Theory predicts negative rotational strength for the L_a region in the far-UV, in contrast to the observed positive CD in this spectral region (Figure 6B). This leads to predicted absolute spectra (*not shown*) that are in poor agreement with experiment. The reasons for this are still not clear, but similar difficulties have been encountered in previous calculations of whole-protein CD. This seems to be most problematic for proteins having substantial amounts of β-sheet structure, e.g., barnase and dihydrofolate reductase (*64*) and pancreatic ribonuclease (*65*). Much better results have been obtained for proteins rich in α-helix (Wollmer, A., Röper, D., Fleischhauer, J., and Woody, R. W., unpublished results). The problems appear to lie mainly in the treatment of the peptide transitions, as has been discussed by Kurapkat et al. (*65*), together with possible remedies.

Analysis of the L_b and L_a rotational strengths reveals evidence for a significant coupling between Tyr 34 and the buried pair, Tyr 56/Tyr 61. The interaction between these groups may account for the absence of a perturbation in the 229 nm CD band upon binding of Y34F g5p to DNA, despite the fact that Tyr 56 is probably the dominant contributor to that band.

SUMMARY

The Y61F g5p, after being refolded in vitro, has nearly normal binding and structural properties as shown by CD titrations and electron microscopy. As g5p is added and binding progresses through multiple binding modes, complexes with g5p undergo partial release of the nucleic acid and changes in the number of g5p dimers and nucleotides per turn of the nucleoprotein helix. We infer from CD difference spectra that a 229 nm protein CD band that is strongly perturbed upon binding may be predominantly due to Tyr 56. Since perturbation of this band fails to occur in a Y34F mutant, changes in the 229 nm band could be the net result of changes in spectral contributions due to a localized perturbation of Tyr 34 (*20*). Our present results suggest an alternative possibility, that Tyr 34 may interact directly or indirectly with the buried Tyr 56 to induce the 229 nm perturbation when complexes are formed with DNA. For two Tyr → Phe mutants in which the Tyr or replacement Phe rings have limited mobility (Y26F and Y34F), we are able to calculate theoretical CD spectra that are in qualitative agreement with experimental spectra. We find that calculated CD spectra are sensitive to small positional changes resulting from energy minimization of the protein. For the Y41F mutant, comparison of calculated and experimental spectra suggests that the structure of g5p in solution may be dominated by Tyr 41 rotamers different from the rotamer stabilized in g5p crystals.

ACKNOWLEDGMENT

We thank Mr. Jun Yuan (Department of Molecular and Cell Biology, The University of Texas at Dallas) for obtaining the 250−320 nm CD spectra of wild-type and Y61F g5p.

SUPPORTING INFORMATION AVAILABLE

One figure, three tables, and supporting discussion. The figure shows CD difference spectra approximating the protein CD components in complexes of Y34F and Y61F g5p with poly[d(A)]. The origins of a CD band in text Figure 6A are discussed. Calculated rotational strengths are given in three tables and described (7 pages). Ordering information is given on any current masthead page.

REFERENCES

1. Model, P., and Russell, M. (1988) in *The Bacteriophages* (Calendar, R. Ed.) pp 386−390, Plenum Press, New York.
2. Alberts, B., Frey, L., and Delius, H. (1972) *J. Mol. Biol. 68*, 139−152.
3. McPherson, A., Jurnak, F., Wang, A., Kopak, F., Molineux, I., and Rich, A. (1978) *Cold Spring Harbor Symp. Quantum Biol. 43*, 21−28.
4. Gray, C. W., Kneale, G. G., Leonard, K. R., Siegrist, H., and Marvin, D. A. (1982) *Virology 116*, 40−52.
5. Gray, C. W. (1989) *J. Mol. Biol. 208*, 57−64.
6. Olah, G. A., Gray, D. M., Gray, C. W., Kergil, D. L., Sosnick, T. R., Mark, B. L., Vaughan, M. R., and Trewhella, J. (1995) *J. Mol. Biol. 249*, 576−594.
7. Gray, D. M., Gray, C. W., and Carlson, R. D. (1982) *Biochemistry 21*, 2702−2713.
8. Skinner, M. M., Zhang, H., Leschnitzer, D. H., Guan, Y., Bellamy, H., Sweet, R. M., Gray, C. W., Konings, R. N. H., Wang, A. H.-J., and Terwilliger, T. C. (1994) *Proc. Natl. Acad. Sci. U.S.A. 91*, 2071−2075.
9. Murzin, A. G. (1993) *EMBO J. 12*, 861−867.
10. Ruff, M., Krishnaswamy, S., Boeglin, M., Poterzman, A., Mitschler, A., Podjarny, A., Rees, B., Thierry, J. C., and Moras, D. (1991) *Science 252*, 1682−1689.
11. Folmer, R. H. A., Nilges, M., Konings, R. N. H., and Hilbers, C. W. (1995) *EMBO J. 14*, 4132−4142.
12. Bochkarev, A., Pfuetzner, R. A., Edwards, A. M., and Frappier, L. (1997) *Nature 385*, 176−181.
13. van Duyenhoven, J. P. M., Folkers, P. J. M., Prinse, C. W. J. M., Harmsen, B. J. M., Konings, R. N. H., and Hilbers, C. W. (1992) *Biochemistry 31*, 1254−1262.
14. Peeters, B. P. H., Konings, R. N. H., and Schoenmakers, J. G. G. (1983) *J. Mol. Biol. 169*, 197−215.
15. King, G. C., and Coleman, J. E. (1987) *Biochemistry 26*, 2929−2937.
16. Folkers, P. J. M., Stassen, A. P. M., van Duynhoven, J. P. M., Harmsen, B. J. M., Konings, R. N. H., and Hilbers, C. W. (1991) *Eur. J. Biochem. 200*, 139−148.
17. King, G. C., and Coleman, J. E. (1988) *Biochemistry 27*, 6947−6953.
18. Stassen, A. P. M., Harmsen, B. J. M., Schoenmakers, J. G. G., Hilbers, C. W., and Konings, R. N. H. (1992) *Eur. J. Biochem. 206*, 605−612.
19. Guan, Y., Zhang, H., Konings, R. N. H., Hilbers, C. W., Terwilliger, T. C., and Wang, A. H.-J. (1994) *Biochemistry 33*, 7768−7778.
20. Mark, B. L., Terwilliger, T. C., Vaughan, M. R., and Gray, D. M. (1995) *Biochemistry 34*, 12854−12865.
21. Terwilliger, T. C., Zabin, H. B., Horvath, M. P., Sandberg, W. S., and Schlunk, P. M. (1994) *J. Mol. Biol. 236*, 556−571.
22. Stassen, A. P. M., Zaman, G. J. R., van Deursen, J. M. A., Schoenmakers, J. G. G., and Konings, R. N. H. (1992) *Eur. J. Biochem. 204*, 1003−1014.
23. Kansy, J. W., Clack, B. A., and Gray, D. M. (1986) *J. Biomol. Struct. Dyn. 3*, 1079−1110.
24. McGhee, J. D., and von Hippel, P. H. (1974) *J. Mol. Biol. 86*, 469−489.
25. Alma, N. C. M., Harmsen, B. J. M., de Jong, E. A. M., van der Ven, J., and Hilbers, C. W. (1983) *J. Mol. Biol. 163*, 47−62.
26. Bulsink, H., Harmsen, B. J. M., and Hilbers, C. W. (1988) *Eur. J. Biochem. 176*, 597−608.
27. Pratt, D., Laws, P., and Griffith, J. (1974) *J. Mol. Biol. 82*, 425−439.
28. Day, L. A. (1973) *Biochemistry 12*, 5329−5339.
29. Manning, M. C., and Woody, R. W. (1991) *Biopolymers 31*, 569−586.
30. Terwilliger, T. C. (1988) *Gene 71*, 41−47.
31. Anderson, R. A., Nakashima, Y., and Coleman, J. E. (1975) *Biochemistry 14*, 907−917.
32. Sambrook, J., Fritsch, E. F., and Maniatis, T. (1989) *Molecular Cloning, A Laboratory Manual*, 2nd ed.; Vol. 3, pp 18.47−18.55. Cold Spring Harbor Laboratory Press.
33. Savitsky, A., and Golay, M. J. E. (1964) *Anal. Chem. 36*, 1627−1639.
34. Gray, C. W. (1994) in *Methods in Molecular Biology, Vol. 30: DNA-Protein Interactions: Principles and Protocols* (Kneale, G. G., Ed.) pp 347−356. Humana Press, NY.
35. Bayley, P. M., Nielsen, E. B., and Schellman, J. A. (1969) *J. Phys. Chem 73*, 228−243.
36. Goux, W. J., and Hooker, T. M. (1980) *J. Am. Chem. Soc. 102*, 7080−7087.
37. Moffitt, W. (1956) *J. Chem. Phys. 25*, 467−478.

38. Brown, A., Kemp, C. M., and Mason, S. F. (1971) *J. Chem. Soc. A* 751−755.
39. Neilsen, E. B., and Schellman, J. A. (1971) *Biopolymers 10*, 1559−1581.
40. Mandel, R., and Holzwarth, G. (1972) *J. Chem. Phys. 57*, 3469−3477.
41. Chen, Y. H., Yang, J. T., and Chan, K. H. (1974) *Biochemistry 13*, 3350−3359.
42. Yamaoka, K., Ueda, K., and Kosako, I. (1986) *J. Am. Chem. Soc. 108*, 4619−4625.
43. Weiner, S. J., Kollman, P. A., Case, D. A., Singh, U. C., Ghio, C., Algona, G., Profeta, S., Jr., and Weiner, P. (1984) *J. Am. Chem. Soc. 106*, 765−784.
44. Mark, B. L., and Gray, D. M. (1997) *Biopolymers 42*, 337−348.
45. Benevides, J. M., Terwilliger, T. C., Vohnik, S., and Thomas, G. J., Jr. (1996) *Biochemistry 35*, 9603−9609.
46. Record, M. T., Jr., Lohman, T. M., and de Haseth, P. (1976) *J. Mol. Biol. 107*, 145−158.
47. Terwilliger, T. C. (1996) *Biochemistry 35*, 16652−16664.
48. Beck, E., Sommer, R., Auerswald, E. A., Kurz, Ch., Zink, B., Osterburg, G., and Schaller, H. (1978) *Nucleic Acids Res. 5*, 4497−4503.
49. Gray, C. W. (1985) in *Fourth Conversation in Biomolecular Stereodynamics* (Sarma, R. H., Ed.) Adenine Press, NY, pp 219−220.
50. Haase-Pettingell, C. A., and King, J. (1988). *J. Biol. Chem. 10*, 4977−4983.
51. Yu, M.-H., and King, J. (1988) *J. Biol. Chem. 263*, 1424−1431.
52. Zabin, H. B., & Terwilliger, T. C. (1991) *J. Mol. Biol. 219*, 257−275.
53. Burley, S. K., and Petsko, G. A. (1985) *Science 229*, 23−28.
54. Johnson, W. C., Jr. (1996) in *Circular Dichroism and the Conformational Analysis of Biomolecules* (Fasman, G. D., Ed.), pp 433−468. Plenum Press, NY.
55. Scheerhagen, M. A., Bokma, J. T., Vlaanderen, C. A., Blok, J., and van Grondelle, R. (1986) *Biopolymers 25*, 1419−1448.
56. Pörschke, D., and Rauh, H. (1983) *Biochemistry 22*, 4737−4745.
57. Sang, B.-C., and Gray, D. M. (1989) *J. Biomol. Struct. Dyn. 7*, 693−706.
58. Shiraki, M. (1969) *Sci. Papers, College Gen. Educ. (University Tokyo) 19*, 151−173.
59. Durand, M., Maurizot, J.-C., Borazan, H. N., and Helène, C. (1975) *Biochemistry 14*, 563−570.
60. Strickland, E. H. (1974) *CRC Crit. Rev. Biochem. 2*, 113−175.
61. Woody, R. W. (1995) *Methods Enzymol. 246*, pp 34−41.
62. Liang, H., and Terwilliger, T. C. (1991) *Biochemistry 30*, 2772−2782.
63. Koslowski, A, Botterweck, H., Fleischhauer, J., Kurapkat, G., Wollmer, A., and Woody, R. W. (1996) *Prog. Biophys. Mol Biol.* 65, Suppl. 1, 43.
64. Grishina, I. B., and Woody, R. W. (1994) *Faraday Discuss. 99*, 245−262.
65. Kurapkat, G., Krüger, P., Wollmer, A., Fleischhauer, J., Kramer, B., Zobel, E., Koslowski, A, Botterweck, H., and Woody, R. W. (1996) *Biopolymers 41*, 267−287.

BI972545K